Chemical Science

RSC Publishing

EDGE ARTICLE

View Article Online
View Journal | View Issue

Cite this: *Chem. Sci.*, 2013, **4**, 3310

Switching the anisotropy barrier of a single-ion magnet by symmetry change from quasi-D_{5h} to quasi-O_h†

Jun-Liang Liu,[a] Yan-Cong Chen,[a] Yan-Zhen Zheng,[b] Wei-Quan Lin,[a] Liviu Ungur,[c] Wolfgang Wernsdorfer,[d] Liviu F. Chibotaru*[c] and Ming-Liang Tong*[a]

Received 28th March 2013
Accepted 9th June 2013

DOI: 10.1039/c3sc50843a

www.rsc.org/chemicalscience

A reversible single-crystal-to-single-crystal transformation is used to dramatically change the relaxation behavior of a single-ion magnet. The coordination geometry of the Dy^{III} site of a [Zn–Dy–Zn] complex changes from pentagonal–bipyramid (quasi-D_{5h}) to octahedron (quasi-O_h), inducing an energy barrier change from 305 cm^{-1} (439 K) to a negligible value, respectively. *Ab initio* calculations reveal that the ideal D_{5h}–Dy^{III} is of perfect axiality with a substantial energy barrier in accordance with the experimental result.

Introduction

Single-ion magnets (SIMs), which contain only one single-spin center that is intriguingly confined in a certain coordination geometry, will slowly relax their magnetization when the magnetic anisotropy energy barrier for magnetization reversal is large with respect to thermal excitations.[1–9] The challenge is to increase the anisotropy barrier in order to yield a high blocking temperature, T_B, below which the bistable magnetization state is stable at a given time scale. This topic attracts a lot of attention for its potential applications in ultra-high density information storage, molecular spintronics, and quantum information processing.[1,2] To advance towards this ultimate goal, several important issues might be addressed, for example, increasing the blocking temperature and switching of exchange couplings inside or between molecules. Here, we establish the switching of the magnetic anisotropy of an SIM. Indeed, lanthanide ions such as Dy^{III}, Tb^{III}, Ho^{III} and Er^{III} can generate huge magnetic anisotropy due to the strong spin–orbital coupling and the crystal field, which depends strongly on the local symmetry.

We focus on the Dy^{III} ion that bears a Kramers spin ground state doublet of its hexadecuplet ($^6H_{15/2}$) making it promising concerning high barrier SIMs.[5,10] Quantum tunneling of magnetization (QTM) is a natural phenomenon which originates from the overlap of wave functions with different spin states.[1a,c] It depends mainly on the crystal-field, intra- and intermolecular interactions, and the hyperfine interaction. The crystal-field effect can be described by the Hamiltonian $\hat{H}_{CF} = \Sigma B_q^k \tilde{O}_q^k$, where the B_q^k are the crystal-field parameters and $\tilde{O}_q^k$ are the Stephen operators. The latter is usually considered as one of the sources of QTM when $q \neq 0$ and $k = 2$, 4, 6, which can significantly reduce the relaxation times in the absence of an external field. It is worth noting that certain parameters B_q^k vanish in high symmetry cases, for example $C_{\infty v}$, $D_{\infty h}$, S_8 (I_4), D_{4d}, D_{5h}, and D_{6d} in theory,[10d] which provides a chemical pathway to control QTM by tuning the local symmetry of the metal centers. So far, SIMs with the first four symmetries ($C_{\infty v}$, $D_{\infty h}$, S_8 (I_4) and D_{4d}) have been realized (Table 1), showing very high energy barriers, in particular the complexes with four-fold symmetry such as the famous $[Ln(Pc)_2]^{0/+/-}$ double-deckers.[4] Inspired by these exciting results, it is therefore of considerable interest to explore the magnetic properties of real complexes with other high symmetries such as D_{5h} and D_{6d}.

Indeed, the D_{5h}-symmetry is achievable using lanthanide ion because of its potential pentagonal–bipyramid geometry when seven coordinated.[11] Herein, we present a delicate synthesis of a Dy^{III} complex with pentagonal–bipyramid and a thermally-activated barrier as large as 305 cm^{-1} (439 K). In addition, this quasi-D_{5h}-core can be nearly reversibly switched into a quasi-O_h-symmetry one *via* single-crystal-to-single-crystal (SCSC) transformation. The latter shows much shorter relaxation times and a negligible energy barrier. *Ab initio* calculations reveal that the quasi-D_{5h} Dy^{III} ion holds a very strong axial magnetic anisotropy, and thus a better SIM behaviour as compared to the less axial quasi-O_h-symmetry one.

[a]*Key Laboratory of Bioinorganic and Synthetic Chemistry of Ministry of Education, State Key Laboratory of Optoelectronic Materials and Technologies, School of Chemistry & Chemical Engineering, Sun Yat-Sen University, 510275 Guangzhou, P. R. China. E-mail: tongml@mail.sysu.edu.cn*

[b]*Center for Applied Chemical Research, Frontier Institute of Science and Technology, Xi'an Jiaotong University, Xi'an 710054, P. R. China*

[c]*Division of Quantum and Physical Chemistry, Department of Chemistry, Katholieke Universiteit Leuven, Celestijnenlaan 200F, 3001 Leuven, Belgium*

[d]*Institut Néel, CNRS & Université Joseph Fournier, BP 166, 25 avenue des Martyrs, 38042 Grenoble Cedex 9, France*

† Electronic supplementary information (ESI) available: Experimental procedures, physical measurements, crystallography, computational details. CCDC 924441 (**1**_as-synthesis), 924442 (**2**), and 924443 (**1**_bath_in_MeOH). For ESI and crystallographic data in CIF or other electronic format see DOI: 10.1039/c3sc50843a

Table 1 The relaxation barrier (H_{dc} = 0 Oe), highest hysteresis temperature and highest AC-peak temperature (H_{dc} = 0 Oe) for selected single-ion magnets

Quasi-symmetry of the Ln^{III} center	Complex	U_{eff} [K] ([cm^{-1}])	Hysteresis temperature [K]	AC-peak temperature [K]	Reference
$D_{\infty h}$	$(C_5Me_5)Er(COT)$	323 (224)	5 (0.00092 T s^{-1})	22–23 (997 Hz)	7*b*
	$[Fe(C(SiMe_3)_3)_2]^-$	325 (226)	4.5 (0.005 T s^{-1})	≤29 (1488 Hz)	9*d*
$D_{4d}/I_4/S_8$	$[ErW_{10}O_{36}]^{9-}$	55.2 (38.3)	—	6.2 (10 000 Hz)	6*a*
	$[Dy(acac)_3(H_2O)_2]$	66.1 (45.9)	0.5 (0.00025 T s^{-1})	12–13 (1488 Hz)	6*c*
	$[Tb(Pc)_2]^-$	374 (260)	1.7[a]	40 (997 Hz)	4*a*,*d*
D_{5h}	[Tb(Pc)(Pc′)]	939 (652)	2[a]	58 (10 000 Hz)	4*e*
	$[Zn_2Dy(L)_2(MeOH)]^+$	439 (305)	11 (0.02 T s^{-1})	29.6 (1488 Hz)	This work

[a] Field sweep rate unknown.

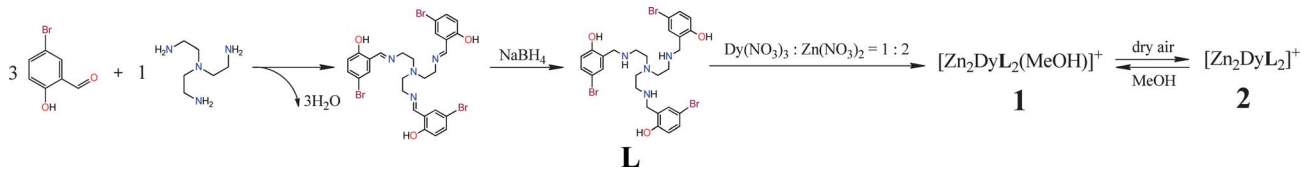

Scheme 1 Synthetic route for **1** and **2**.

Results and discussion

By careful selection we used a tripodal ligand, 2,2′,2″-(((nitrilotris(ethane-2,1-diyl))tris(azanediyl))tris(methylene))tris-(4-bromophenol) (**L**), which can be synthesized from the condensation of 5-bromo-salicylaldehyde and tris(2-aminoethy1)amine (3 : 1), followed by the reduction using $NaBH_4$ (Scheme 1) for this symmetry design. Subsequently, **L** was used to react with both zinc and dysprosium nitrates with stoichiometry (2 : 1) in methanol, leading to the formation of crystalline solid $[Zn_2DyL_2(MeOH)]NO_3\cdot 3MeOH\cdot H_2O$ (**1**). Very interestingly, if **1** is exposed to the dry air for one day it loses its coordinated methanol molecule but retains its crystallinity. X-ray diffraction shows a composition of $[Zn_2DyL_2]NO_3\cdot H_2O$ (**2**), which can convert back to **1** after soaking in methanol for one day (see ESI† for details concerning the SCSC transformation).

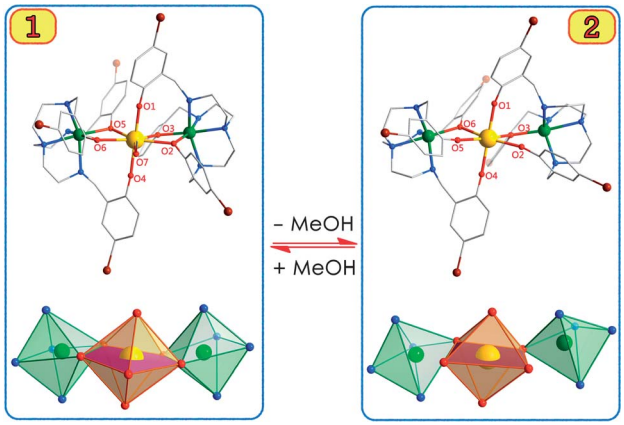

Fig. 1 Structural motifs of the [Zn–Dy–Zn] cores of **1** and **2**. The Dy^{III} is highlighted as orange polyhedrons. Yellow, green, gray, red, blue and brown spheres represent Dy, Zn, C, O, N and Br, respectively. Hydrogen atoms have been omitted for clarity.

The X-ray single crystal structure analysis reveals that the seven coordination sites of the Dy^{III} ions are all occupied by oxygen atoms, whereas the Zn^{II} ions sit in a four-nitrogen "pocket" of the tripodal ligand **L** in both complexes (Fig. 1). For **1**, each of the six-coordinate Zn^{II} octahedra is completed by two bridging phenoxyl groups, which give in total four oxygen atoms to the pentagonal plane of the central Dy^{III} (Table 2 and S2†). The remaining oxygen of the pentagon is from a terminal methanol ligand. The axial pentagonal–bipyramid geometry of the Dy^{III} is further completed by two phenoxyl oxygen atoms. When the terminal methanol leaves, two of the bridging phenoxyl groups get closer to the Dy^{III} rather than to the Zn^{II}, which changes the coordination-geometry. The program SHAPE 2.0 (ref. 12) was used to analyze the coordination geometries of the metal ions. Table S3† reveals that both the coordination geometries of Dy^{III} and Zn^{II} are changed after transformation: concerning Dy^{III} from pentagonal–bipyramid (quasi-D_{5h}) to octahedron (quasi-O_h), and concerning Zn^{II} from octahedron (quasi-O_h) to distorted trigonal–bipyramid (quasi-D_{3h}, τ = 0.69–0.70). In addition, the distance between nearest neighboring clusters is *ca.* 10.46 Å and 9.23 Å for **1** and **2**, respectively (Fig. S2†), because of different hydrogen bonding among clusters, nitrate, MeOH and H_2O motifs.

Temperature-dependent direct-current (DC) susceptibilities of both **1** and **2** were performed. At room temperature the $\chi_M T$ products for **1** and **2** are nearly identical, *ca.* 13.8 cm^3 K mol^{-1} (Fig. 2), which is slightly smaller than the expected value (14.2 cm^3 K mol^{-1}) for the $^6H_{15/2}$ state.[10a,b] The $\chi_M T$ products descend very slowly upon cooling, which is a typical behavior for a 4*f* paramagnetic ion due to the depopulation of Stark sublevels. The very small declines of the $\chi_M T$ products suggest that the excited Kramers doublets are very high above the ground one.

Table 2 Selected bond lengths (Å) and angles (°) of Dy^{III} for **1** and **2**

	1 as-synthesis		**2**		**1** bath in MeOH	
Dy–O bond lengths	Dy1–O1	2.195(7)	Dy1–O1	2.183(7)	Dy1–O1	2.137(11)
	Dy1–O2	2.397(6)	Dy1–O2	2.228(8)	Dy1–O2	2.413(10)
	Dy1–O3	2.366(6)	Dy1–O3	2.377(7)	Dy1–O3	2.367(10)
	Dy1–O4	2.221(6)	Dy1–O4	2.189(8)	Dy1–O4	2.195(11)
	Dy1–O5	2.402(6)	Dy1–O5	2.196(8)	Dy1–O5	2.393(9)
	Dy1–O6	2.375(6)	Dy1–O6	2.389(7)	Dy1–O6	2.388(10)
	Dy1–O7	2.427(6)			Dy1–O7	2.445(9)
O–Dy–O bond angles	O1–Dy1–O2	83.4(3)	O1–Dy1–O2	87.1(3)	O1–Dy1–O2	83.0(4)
	O1–Dy1–O3	96.6(3)	O1–Dy1–O3	92.2(3)	O1–Dy1–O3	95.6(4)
	O1–Dy1–O4	168.6(2)	O1–Dy1–O4	173.1(3)	O1–Dy1–O4	169.3(3)
	O1–Dy1–O5	94.4(2)	O1–Dy1–O5	91.3(3)	O1–Dy1–O5	94.3(3)
	O1–Dy1–O6	90.3(3)	O1–Dy1–O6	91.0(2)	O1–Dy1–O6	90.9(3)
	O1–Dy1–O7	87.5(2)			O1–Dy1–O7	87.4(4)
	O4–Dy1–O2	93.9(2)	O4–Dy1–O2	90.2(3)	O4–Dy1–O2	94.0(4)
	O4–Dy1–O3	92.6(2)	O4–Dy1–O3	93.7(3)	O4–Dy1–O3	92.6(4)
	O4–Dy1–O5	94.3(2)	O4–Dy1–O5	84.3(3)	O4–Dy1–O5	94.3(3)
	O4–Dy1–O6	86.3(2)	O4–Dy1–O6	93.4(2)	O4–Dy1–O6	86.4(3)
	O4–Dy1–O7	81.1(2)			O4–Dy1–O7	81.8(4)
	O2–Dy1–O3	68.4(2)	O2–Dy1–O3	80.8(3)	O2–Dy1–O3	67.0(3)
	O3–Dy1–O5	76.2(2)	O3–Dy1–O6	83.0(2)	O3–Dy1–O5	76.6(3)
	O5–Dy1–O6	67.0(2)	O6–Dy1–O5	78.5(3)	O5–Dy1–O6	67.6(3)
	O6–Dy1–O7	75.4(2)	O5–Dy1–O2	117.8(3)	O6–Dy1–O7	75.9(3)
	O7–Dy1–O2	73.7(2)			O7–Dy1–O2	73.5(3)

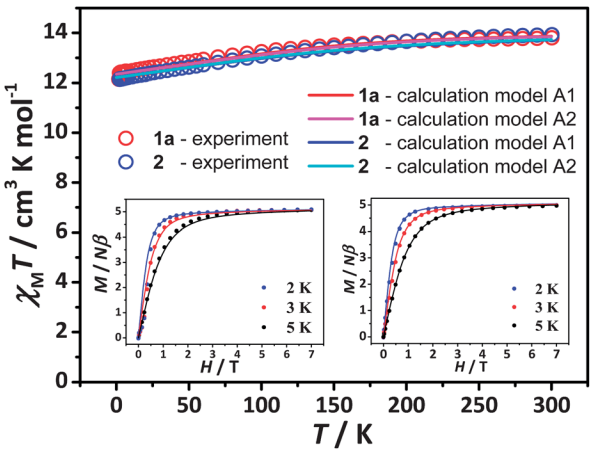

Fig. 2 Temperature dependence of $\chi_M T$ products at 100 Oe for **1** (black) and **2** (blue). Inset: plots of *M*–*H* for **1** (*left*) and **2** (*right*) at 2, 3 and 5 K. The solid lines correspond to *ab initio* calculations.

The magnetization increases very fast at low fields, indicating the very well separated excited Kramers doublets, and it reaches the "saturation" of 5.09 $N\beta$ for **1** and 4.99 $N\beta$ for **2**.

Alternating-current (AC) susceptibility measurements were also performed (Fig. 3, S3 and S4†). In zero DC field, the out-of-phase susceptibilities for **1** exhibit a strong frequency-dependent behaviour below 30 K. The relaxation time (τ) can be extracted from both temperature- and frequency-dependent susceptibilities (Fig. 4). In the high-temperature regime, the relaxation process of **1** follows an Arrhenius law with an effective energy barrier $U_{eff} = 305 \pm 3$ cm^{-1} (439 ± 5 K), which is consistent with the value (294.8 cm^{-1}, 424.6 K) determined by *ab initio*

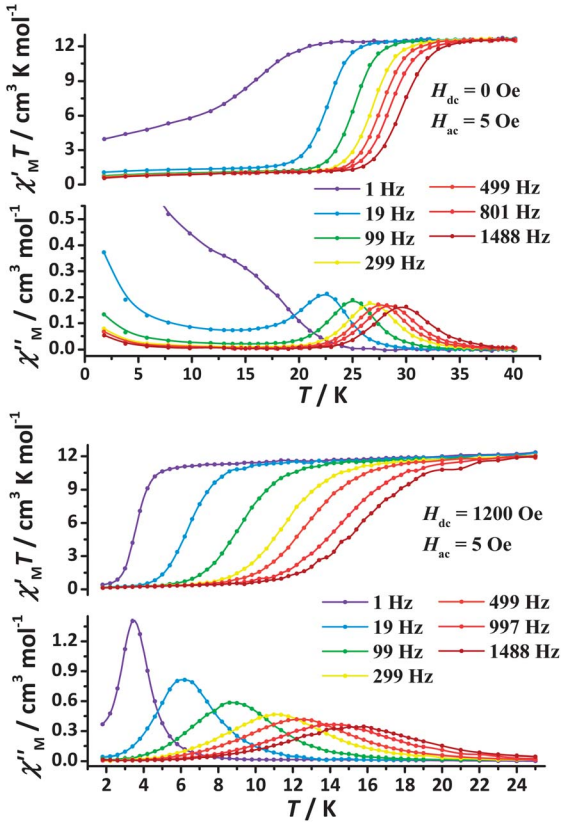

Fig. 3 Plots of the susceptibility *vs.* temperature at frequencies between 1 and 1488 Hz at $H_{dc} = 0$ Oe ($H_{ac} = 5$ Oe) for **1** (*top*) and $H_{dc} = 1200$ Oe ($H_{ac} = 5$ Oe) for **2** (*bottom*), respectively.

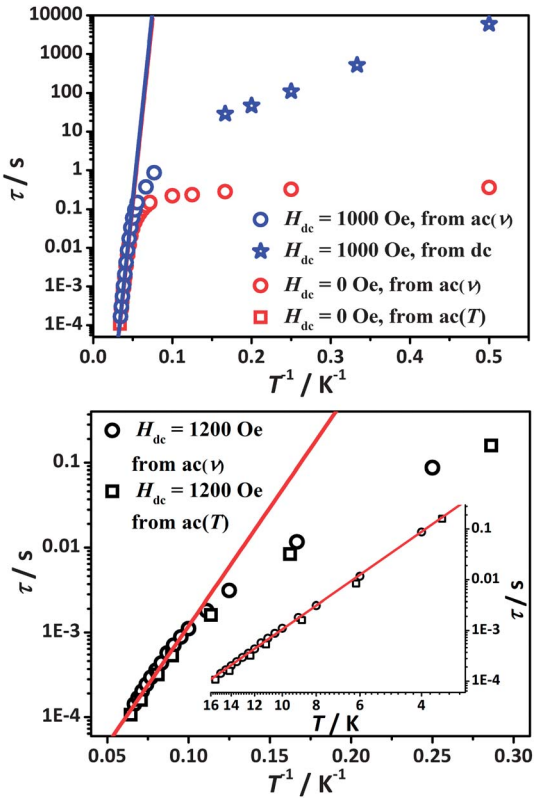

Fig. 4 *Top*: the relaxation time τ (logarithmic scale) *vs.* T^{-1} plots obtained from $\chi_M'(T)$, $\chi_M'(\nu)$ and dc magnetization relaxation for **1**. The solid lines correspond to an Arrhenius law; *bottom*: the relaxation time τ (logarithmic scale) *vs.* T^{-1} plots obtained from $\chi_M'(T)$ and $\chi_M'(\nu)$ for **2**. Inset: the relaxation time τ (logarithmic scale) *vs.* T (logarithmic scale) plots for **2**. The solid lines respectively correspond to an Arrhenius law and a power law.

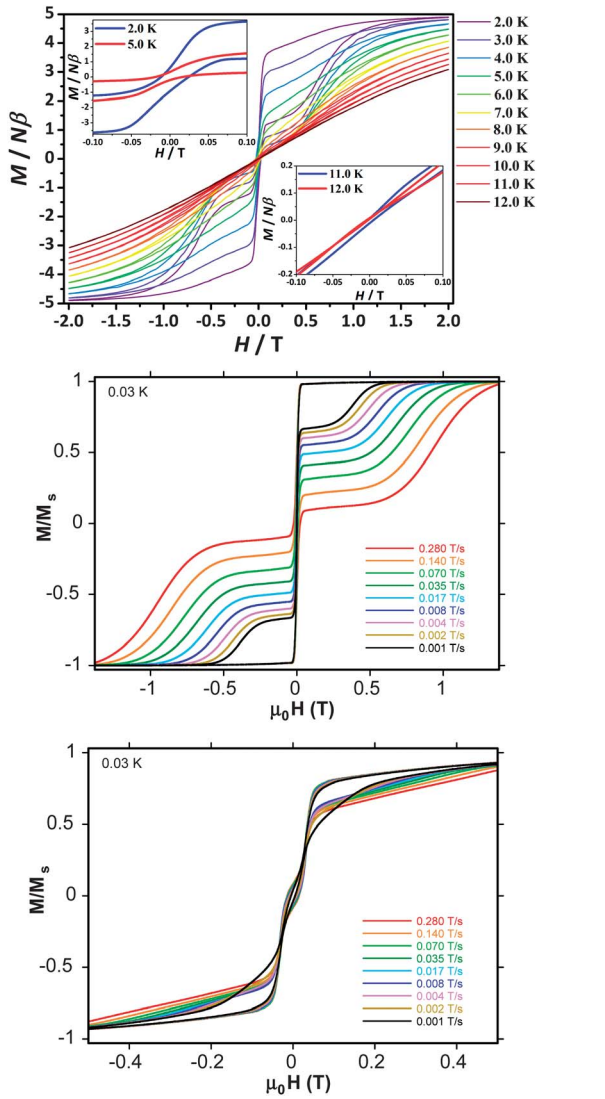

Fig. 5 Magnetization measurements *vs.* applied field for the powder sample for **1** (*top*) at a sweep rate of 0.02 T s^{-1} and the indicated temperatures, and for the single crystal samples of **1** (*middle*) and **2** (*bottom*) at 0.03 K and the indicated field sweep rates.

calculations (*vide infra*). The large energy barrier may be attributed to the local quasi-D_{5h} symmetry of the Dy^{III} ion as well as the interaction with two very close phenoxyls coordinating axially.[4c,5,7b,8] The AC-peak temperature (T_m) and the effective energy barrier for **1** are one of the highest among SIMs (Table 1).

Quantum tunnelling of magnetization, which mainly originates from the crystal-field effect for the departure of an ideal D_{5h} local symmetry, comes into play at low temperatures ($\tau_{@2K} = 0.36$ s) (*vide infra*). Under an external field of 1000 Oe (Fig. S3 and S5†), the relaxation time increases strongly at low temperatures ($\tau_{@2K} = 6000$ s, Fig. S6†) because of the suppression of QTM between the states of the Kramers ground doublet.

Because the relaxation time becomes very long at low temperatures, hysteresis loops were observed. For this reason, temperature-dependent hysteresis loops are observed for the powder sample under a scan rate of 0.02 T s^{-1} and for a single crystal (Fig. 5 and S7†). Concerning the latter, the field was aligned with the easy axis of the crystal using a micro-SQUID magnetometer and the transverse field method.[13] It was not possible to relate the easy axis of the crystal with the crystallographic axes. The observed hysteresis loops are typical for SIMs, that is, they are butterfly loops with a fast tunnel step at zero field. For complex **1**, the loops are clearly open up below 11 K at a scan rate of 0.02 T s^{-1}, which is the highest among all reported SIMs to our knowledge (Table 1), close to that of the radical-bridged $\{Tb_2\}$ single-molecule magnet by Long and co-workers.[14] Note that complex **2** shows a small antiferromagnetic exchange coupling between molecules (seen by the shift of the zero-field resonance to negative/positive fields, Fig. 5), which is in accordance with the closer nearest neighbouring clusters distance of **2**.

With the local symmetry of Dy^{III} changing from quasi-D_{5h} to quasi-O_h by desolvating, a dramatic change of the relaxation times is observed, in particular, complex **2** does not show a peak of χ_M'' at zero applied field (Fig. S4†), which is due to very fast tunneling effects. However, when applying an optimized field of 1200 Oe (Fig. S4 and S8†), the peaks of χ_M'' are observed below 15.0 K (1488 Hz), whose T_m are much smaller than that of the pentagonal–bipyramid one. We found that the relaxation times obey a power law ($\tau \sim T^{-n}$; $n = 4.83 \pm 0.03$) instead of an Arrhenius (exponential) law in the studied temperature range (Fig. 4), which is indicative that compound **2** involves an admixture of direct and Raman

Table 3 Energies of the low-lying Kramers doublets and the corresponding *ab initio* calculated parameters of the crystal field B_q^k in **1** and **2**

		B_q^k parameters		*Ab initio* energies (cm^{-1})	
k	q	**1**	**2**	**1**	**2**
2	−2	0.254	−1.99	0.0	0.0
	−1	0.806	1.19	289.9	294.8
	0	**−1.72**	**−2.48**	303.3	330.4
	1	0.573	1.13	369.4	413.5
	2	1.37	**3.11**	433.4	491.7
				464.0	560.2
4	−4	0.205×10^{-2}	$\mathbf{-0.429 \times 10^{-1}}$	504.3	710.0
	−3	-0.154×10^{-2}	0.106×10^{-2}	542.5	838.4
	−2	-0.364×10^{-3}	0.259×10^{-2}		
	−1	-0.644×10^{-2}	-0.787×10^{-2}	*g*-Tensor of the ground	
	0	$\mathbf{-0.114 \times 10^{-1}}$	$\mathbf{-0.126 \times 10^{-1}}$	Kramers doublet	
	1	-0.282×10^{-2}	-0.855×10^{-2}	$g_X = 0.00$	$g_X = 0.01$
	2	-0.562×10^{-3}	-0.529×10^{-2}	$g_Y = 0.00$	$g_Y = 0.01$
	3	-0.939×10^{-2}	$\mathbf{-0.110 \times 10^{-1}}$	$g_Z = 19.87$	$g_Z = 19.76$
	4	0.285×10^{-2}	0.671×10^{-2}		
6	−6	-0.262×10^{-4}	-0.251×10^{-4}		
	−5	0.283×10^{-4}	-0.953×10^{-4}		
	−4	-0.109×10^{-4}	$\mathbf{-0.220 \times 10^{-3}}$		
	−3	0.893×10^{-5}	0.393×10^{-4}		
	−2	0.118×10^{-4}	0.101×10^{-4}		
	−1	0.208×10^{-4}	0.778×10^{-5}		
	0	0.570×10^{-5}	0.171×10^{-4}		
	1	-0.221×10^{-4}	0.172×10^{-4}		
	2	0.234×10^{-4}	-0.411×10^{-4}		
	3	-0.710×10^{-4}	-0.180×10^{-4}		
	4	-0.175×10^{-4}	0.312×10^{-4}		
	5	0.332×10^{-4}	0.220×10^{-3}		
	6	-0.285×10^{-4}	-0.259×10^{-5}		

processes rather than an Orbach process,[10a,c,15] similar to a recently reported 6-coordinate field-induced SIM.[16] The obtained "apparent energy barrier" in the high-temperature regime of $U_{app} = 44 \pm 2$ cm^{-1} (64 ± 2 K) is an order of magnitude smaller than the first excited Kramers doublets, determined from *ab initio* calculations (294.8 cm^{-1}, 424.6 K). This huge difference further excludes an Orbach process for **2**. The hysteresis loops of the powder sample (Fig. S9†) has an almost negligible coercivity due to the short zero-field relaxation time ($\tau_{@3.5K} = 0.16$ s). The small α parameters ($\alpha_{1@0\,Oe} = 0.09$–0.11; $\alpha_{1@1000\,Oe} = 0.04$–$0.05$; $\alpha_{2@1200\,Oe} = 0.02$–$0.06$) obtained from the semicircular Cole–Cole plots (Fig. S10 and S11†) reveal very narrow distribution of the relaxation process.[17]

In order to get further insight into the low-lying electronic structure and the magnetic anisotropy on the Dy^{III} site, *ab initio* calculations of the CASSCF/RASSI/SINGLE_ANISO type[18a] on the experimental structures were performed (Table 3 and Fig. 6). The details of these calculations are given in the ESI.† A recent development of the SINGLE_ANISO software allows for *ab initio* calculation of the crystal-field parameters in lanthanide complexes:

$$\hat{H}_{CF} = \sum \sum_{k=-q}^{q} B_q^k \tilde{O}_q^k \quad (1)$$

where $\tilde{O}_q^k$ are the extended Stevens operators.[18b,c] Table 3 shows the computed B_q^k parameters for **1** and **2**. The *g*-tensor of the ground doublet state is the main characteristic defining whether the complex will be an SIM or not. In order to understand the influence of geometrical deviations from the ideal symmetry, D_{5h} for **1** and O_h for **2**, on the magnetic blocking in these complexes, we did similar calculations for the two limiting idealized cases: the pentagonal bipyramid $Dy(OCH)_7^{4-}$ and the octahedron $Dy(OCH)_6^{3-}$ (see the ESI†). Even if the real complexes both deviate from their corresponding ideal geometries, the difference in the anisotropic properties of their

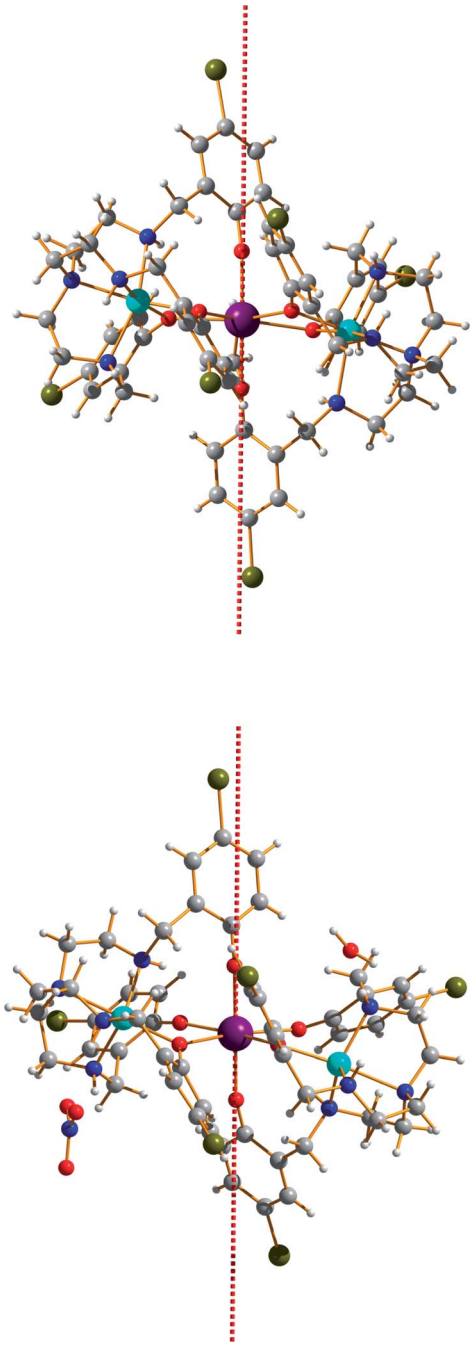

Fig. 6 Orientation of the main anisotropy axes in the ground Kramers doublet of **1** (*top*) and **2** (*bottom*) obtained in computational approximations A2. Violet, indigo, gray, red, blue and dark yellow spheres represent Dy, Zn, C, O, N and Br, respectively.

ground states is not accidental but can be naturally explained by the genealogy of their structure.

We found that the crystal-field parameters, causing the splitting of the low-lying $J = 15/2$ multiplet in **1** and **2** (Table 3), differ significantly from their idealized fragments (Table S13†). The blocking properties in the latter are simply understandable. The ground Kramers doublet in pentagonal bipyramid is characterized $g_X = g_Y = 0$, *i.e.*, by a perfect axiality expected for its irreducible representation $E_{3/2}$ of D_{5h} symmetry group (see Table II in ref. 18*d*). This means that QTM will be completely suppressed in this state and the complex is expected to be a good SIM. The departure from D_{5h} symmetry in **1** reduces its SIM performance.

On the contrary, the Kramers ground doublet in the ideal octahedron is completely isotropic, with $g_X = g_Y = g_Z = 6.58$ (Table S13†), and this leads to a very fast relaxation of magnetization. However, the departure from ideal octahedral symmetry yields low-symmetry terms of the crystal field, which give to **2** some magnetic anisotropy and hence a certain slow relaxation. In other words, the low-symmetry crystal field has opposite effects in **1** and **2**. Nevertheless, despite a significant departure from the respective idealized geometry, **1** still remains much more axial than **2**. This is reflected in the fact that in **1** the axial parameters (B_0^2, B_0^4) are the largest, while in **2** the non-axial parameters (B_2^2, B_4^4, B_3^4) are of the same order or even larger than the axial ones (Table 3). As a result, the *g*-tensor in **1** is still strongly axial resulting in suppression of QTM, while in **2** the transverse components g_X and g_Y are larger, which is the reason why this complex does not show slow relaxation of magnetization without applying a DC magnetic field.

Conclusions

To summarize, we have successfully isolated a Dy^{III} SIM (complex **1**) with quasi-D_{5h} symmetry, which exhibits a large thermally activated barrier with long relaxation times. The desolvation of **1** altered the local symmetry to quasi-O_h. This new complex **2** possesses thus a much lower energy barrier. Interestingly, in response to the solvent, the complex **2** can be converted back to **1** *via* an SCSC transformation. *Ab initio* calculations reveal that the ideal D_{5h}–Dy^{III} is of perfect axiality with a substantial energy barrier in accordance to the experimental result. This work demonstrates that the SCSC transformation offers an important tool to investigate the importance of the local symmetry on the performance of SIMs. It hints at a promising way to improve SIMs by the proper choice of the complex symmetries such as D_{5h}, in particular by avoiding crystal-field terms B_q^k ($q \neq 0$).

Acknowledgements

This work was supported by the "973 Project" (2012CB821704) and the NSFC (Grant no. 91122032, 21121061, J1103305 and 21201137) and ERC Advanced Grant MolNanoSpin no. 226558. L. U. is a post-doc of the Fonds Wetenschappelijk Onderzoek-Vlaanderen and also gratefully acknowledges INPAC and Methusalem grants of KU Leuven.

Notes and references

1 (*a*) D. Gatteschi, R. Sessoli and J. Villain, *Molecular Nanomagnets*, 2006, pp. 1, 182, 216; (*b*) A. Dei and D. Gatteschi, *Angew. Chem., Int. Ed.*, 2011, **50**, 11852; (*c*) D. Gatteschi and R. Sessoli, *Angew. Chem., Int. Ed.*, 2003, **42**, 268; (*d*) M. N. Leuenberger and D. Loss, *Nature*, 2001, **410**, 789; (*e*) W. Wernsdorfer and R. Sessoli, *Science*, 1999, **284**, 133.

2 (*a*) L. Bogani and W. Wernsdorfer, *Nat. Mater.*, 2008, **7**, 179; (*b*) M. Mannini, F. Pineider, P. Sainctavit, C. Danieli, E. Otero, C. Sciancalepore, A. M. Talarico, M.-A. Arrio, A. Cornia, D. Gatteschi and R. Sessoli, *Nat. Mater.*, 2009, **8**, 194; M. Ganzhorn, S. Klyatskaya, M. Ruben and W. Wernsdorfer, *Nat. Nanotechnol.*, 2013, **8**, 165.

3 (*a*) R. Sessoli, D. Gatteschi, A. Caneschi and M. A. Novak, *Nature*, 1993, **365**, 141; (*b*) R. Sessoli, H. L. Tsai, A. R. Schake, S. Wang, J. B. Vincent, K. Folting, D. Gatteschi, G. Christou and D. N. Hendrickson, *J. Am. Chem. Soc.*, 1993, **115**, 1804.

4 (*a*) N. Ishikawa, M. Sugita, T. Ishikawa, S.-y. Koshihara and Y. Kaizu, *J. Am. Chem. Soc.*, 2003, **125**, 8694; (*b*) N. Ishikawa, M. Sugita and W. Wernsdorfer, *Angew. Chem., Int. Ed.*, 2005, **44**, 2931; (*c*) S. Takamatsu, T. Ishikawa, S. y. Koshihara and N. Ishikawa, *Inorg. Chem.*, 2007, **46**, 7250; (*d*) N. Ishikawa, M. Sugita, T. Ishikawa, S. Koshihara and Y. Kaizu, *J. Phys. Chem. B*, 2004, **108**, 11265; (*e*) C. R. Ganivet, B. Ballesteros, G. de la Torre, J. M. Clemente-Juan, E. Coronado and T. Torres, *Chem.–Eur. J.*, 2013, **19**, 1457.

5 (*a*) J. D. Rinehart and J. R. Long, *Chem. Sci.*, 2011, **2**, 2078; (*b*) L. Sorace, C. Benelli and D. Gatteschi, *Chem. Soc. Rev.*, 2011, **40**, 3092; (*c*) D. Gatteschi, *Nat. Chem.*, 2011, **3**, 830; (*d*) D. N. Woodruff, R. E. P. Winpenny and R. A. Layfield, *Chem. Rev.*, 2013, DOI: 10.1021/cr400018q.

6 (*a*) M. A. AlDamen, J. M. Clemente-Juan, E. Coronado, C. Martí-Gastaldo and A. Gaita-Ariño, *J. Am. Chem. Soc.*, 2008, **130**, 8874; (*b*) M.-E. Boulon, G. Cucinotta, J. Luzon, C. Degl'Innocenti, M. Perfetti, K. Bernot, G. Calvez, A. Caneschi and R. Sessoli, *Angew. Chem., Int. Ed.*, 2013, **52**, 350; (*c*) S.-D. Jiang, B.-W. Wang, G. Su, Z.-M. Wang and S. Gao, *Angew. Chem., Int. Ed.*, 2010, **49**, 7448.

7 (*a*) R. Westerström, J. Dreiser, C. Piamonteze, M. Muntwiler, S. Weyeneth, H. Brune, S. Rusponi, F. Nolting, A. Popov, S. Yang, L. Dunsch and T. Greber, *J. Am. Chem. Soc.*, 2012, **134**, 9840; (*b*) S. D. Jiang, B. W. Wang, H. L. Sun, Z. M. Wang and S. Gao, *J. Am. Chem. Soc.*, 2011, **133**, 4730; (*c*) M. Jeletic, P.-H. Lin, J. J. Le Roy, I. Korobkov, S. I. Gorelsky and M. Murugesu, *J. Am. Chem. Soc.*, 2011, **133**, 19286; (*d*) N. Magnani, C. Apostolidis, A. Morgenstern, E. Colineau, J.-C. Griveau, H. Bolvin, O. Walter and R. Caciuffo, *Angew. Chem., Int. Ed.*, 2011, **50**, 1696.

8 (*a*) H. L. C. Feltham, Y. Lan, F. Klöwer, L. Ungur, L. F. Chibotaru, A. K. Powell and S. Brooker, *Chem.–Eur. J.*, 2011, **17**, 4362; (*b*) A. Yamashita, A. Watanabe, S. Akine, T. Nabeshima, M. Nakano, T. Yamamura and T. Kajiwara, *Angew. Chem., Int. Ed.*, 2011, **50**, 4016.

9 (*a*) J. M. Zadrozny, M. Atanasov, A. M. Bryan, C.-Y. Lin, B. D. Rekken, P. P. Power, F. Neese and J. R. Long, *Chem. Sci.*, 2013, **4**, 125; (*b*) J. D. Rinehart and J. R. Long, *J. Am. Chem. Soc.*, 2009, **131**, 12558; (*c*) Y.-Y. Zhu, C. Cui, Y.-Q. Zhang, J.-H. Jia, X. Guo, C. Gao, K. Qian, S.-D. Jiang, B.-W. Wang, Z.-M. Wang and S. Gao, *Chem. Sci.*, 2013, **4**, 1802; (*d*) J. M. Zadrozny, D. J. Xiao, M. Atanasov, G. J. Long, F. Grandjean, F. Neese and J. R. Long, *Nat. Chem.*, 2013, DOI: 10.1038/nchem.1630.

10 (*a*) R. L. Carlin, *Magnetochemistry*, Springer-Verlag, 1986; (*b*) O. Kahn, *Molecular Magnetism*, Wiley-VCH, New York, 1993; (*c*) A. Abragam and B. Bleaney, *Electron Paramagnetic Resonance of Transition Ions*, Oxford University Press, 1970; (*d*) C. Görller-Walrand, K. Binnemans, K. A. Gschneidner and L. Eyring, *Handbook on the Physics and Chemistry of Rare Earths*, 1996, vol. 23.

11 (*a*) G. Novitchi, S. Shova, A. Caneschi, J.-P. Costes, M. Gdaniec and N. Stanica, *Dalton Trans.*, 2004, 1194; (*b*) S. R. Bayly, Z. Xu, B. O. Patrick, S. J. Rettig, M. Pink, R. C. Thompson and C. Orvig, *Inorg. Chem.*, 2003, **42**, 1576; (*c*) Y.-N. Guo, G.-F. Xu, W. Wernsdorfer, L. L. Ungur, Y. Guo, J. Tang, H.-J. Zhang, L. F. Chibotaru and A. K. Powell, *J. Am. Chem. Soc.*, 2011, **133**, 11948.

12 (*a*) S. Alvarez, P. Alemany, D. Casanova, J. Cirera, M. Llunell and D. Avnir, *Coord. Chem. Rev.*, 2005, **249**, 1693; (*b*) D. Casanova, P. Alemany, J. M. Bofill and S. Alvarez, *Chem.–Eur. J.*, 2003, **9**, 1281; (*c*) S. Alvarez, D. Avnir, M. Llunell and M. Pinsky, *New J. Chem.*, 2002, **26**, 996; (*d*) S. Alvarez and M. Llunell, *J. Chem. Soc., Dalton Trans.*, 2000, 3288.

13 (*a*) W. Wernsdorfer, N. E. Chakov and G. Christou, *Phys. Rev. B: Condens. Matter Mater. Phys.*, 2004, **70**, 132413; (*b*) W. Wernsdorfer, *Supercond. Sci. Technol.*, 2009, **22**, 064013.

14 J. D. Rinehart, M. Fang, W. J. Evans and J. R. Long, *J. Am. Chem. Soc.*, 2011, **133**, 14236.

15 (*a*) A. Singh and K. N. Shrivastava, *Phys. Status Solidi B*, 1979, **95**, 273; (*b*) K. N. Shrivastava, *Phys. Status Solidi B*, 1983, **117**, 437.

16 J.-L. Liu, K. Yuan, J.-D. Leng, L. Ungur, W. Wernsdorfer, F.-S. Guo, L. F. Chibotaru and M.-L. Tong, *Inorg. Chem.*, 2012, **51**, 8538.

17 K. S. Cole and R. H. Cole, *J. Chem. Phys.*, 1941, **9**, 34.

18 (*a*) F. Aquilante, L. De Vico, N. Ferre, G. Ghigo, P.-A. Malmqvist, P. Neograd y, T. B. Pedersen, M. Pitonak, M. Reiher, B. O. Roos, L. Serrano-Andres, M. Urban, V. Veryazov and R. Lindh, *J. Comput. Chem.*, 2010, **31**, 224; (*b*) C. Rudowicz and C. Y. Chung, *J. Phys.: Condens. Matter*, 2004, **16**, 5825; (*c*) L. F. Chibotaru and L. Ungur, *J. Chem. Phys.*, 2012, **137**, 064112; (*d*) L. Ungur and L. F. Chibotaru, *Phys. Chem. Chem. Phys.*, 2011, **13**, 20086; Erratum: idem, 21658.

